



This is the accepted manuscript made available via CHORUS. The article has been published as:

# Emergent superconductivity and non-Fermi liquid transport in a doped valence bond solid insulator

Zi-Xiang Li, Steven G. Louie, and Dung-Hai Lee Phys. Rev. B **107**, L041103 — Published 11 January 2023

DOI: 10.1103/PhysRevB.107.L041103

## Emergent superconductivity and non-Fermi liquid transport in a doped valence bond solid insulator

Zi-Xiang Li, Steven G. Louie, and Dung-Hai Lee\*

Department of Physics, University of California, Berkeley, CA 94720, USA.

Materials Sciences Division, Lawrence Berkeley National Laboratory, Berkeley, CA 94720, USA.

In this paper, we study the superconductivity and non-Fermi liquid transport behavior in a doped valence bond solid insulator using sign-problem-free Quantum Monte Carlo simulation. We show superconductivity emerges as a function of doping. For a wide temperature range above the superconducting  $T_c$  a pseudogap exists. Moreover, close to the valence bond solid to semimetal quantum critical point at half filling, we observe linear temperature resistivity when doping is non-zero.

#### Introduction

In 1986 P.W. Anderson proposed the resonating valence bond (RVB) mechanism for the hightemperature superconductivity discovered in copperoxides (cuprates)[1]. In Anderson's theory, the spins form an RVB liquid at half-filling. Doping injects charged holons which condense in the superconducting state. When the doping density is low the superconductor has a low superfluid density. This proposal has influenced condensed matter physics greatly [2, 3]. The notion of a spin liquid is regarded as a quantum paramagnetic state with topological order and anyon excitations [4–7]. Although there are concrete theoretical examples of spin liquid [8– 10, experimentally a magnetic material that has been unambiguously established to be a spin liquid is yet to be achieved. Concerning RVB, recently a density matrix renormalization group calculation done on 6-leg t-J ladders finds d-wave superconducting pairing emerging from doping a quantum paramagnet, which supports the RVB proposal[11].

On a different front, valence bonds may freeze into the valence bond solid (VBS) phase. The VBS phase has been established in various theoretical models[12–14] and realistic materials[15–21]. Remarkably, there exists a VBS material which becomes superconducting when VBS order is suppressed by pressure[18]. Hence, it is an intriguing question is whether superconductivity can emerge from doping a VBS phase.

In this paper, we carried out a numerically exact quantum Monte-Carlo (QMC) simulation [22, 27] to study a doped VBS on the honeycomb lattice. (See section I. of the Supplemental Materials (SM) for details of the simulation. [28]) At half-filling, as a function of an interaction parameter (the P in Eq. (1)), the system goes from a semimetal phase to an insulating VBS phase (see Fig. 3(c)). Here the "valence bond" refers to that of Pauling (in Benzene), rather than the Heitler-London singlet bond in RVB. Our results show that the presence of doping mobile holes destroys the VBS order in favor of superconductivity. At finite temperatures, there is a Kosterlitz-Thouless transition. In a wide temperature range above the superconducting transition, there is a

pseudogap. Moreover, when the interaction parameter is close to the critical value for the VBS to semimetal transition, we observed non-Fermi liquid transport behavior. In the rest of the paper, we detail the above findings.

#### The model

We consider the following model of spin-1/2 fermions

$$H = H_0 + H_1$$

$$H_0 = -t \sum_{\langle ij \rangle, \sigma} \left( \psi_{i\sigma}^{\dagger} \psi_{j\sigma} + h.c. \right) - \mu \sum_{i\sigma} \psi_{i\sigma}^{\dagger} \psi_{i\sigma}$$

$$H_1 = -\frac{P}{4} \sum_{\Omega} (A_{\Omega}^2 + B_{\Omega}^2)$$
(1)

Here,  $\psi_{i,\sigma}$  annihilates an electron with spin  $\sigma$  on the hon-

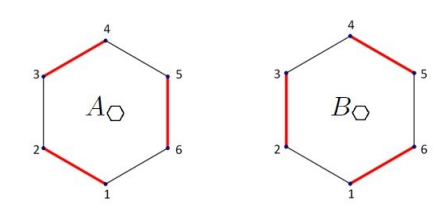


FIG. 1. The four-fermion term associated with each hexagonal plaquette in  $H_1$ . The red line represents the hopping terms in Eq. (2).

eycomb lattice site i, t is the nearest-neighbor hopping amplitude and  $\mu$  is chemical potential. Hereafter, we fix t = 1 as unit of energy.  $H_1$  in Eq. (1) is a four-fermion term defined for each plaquette [29], where

$$A_{\bigcirc} = \sum_{\sigma} (\psi_{1\sigma}^{\dagger} \psi_{2\sigma} + \psi_{3\sigma}^{\dagger} \psi_{4\sigma} + \psi_{5\sigma}^{\dagger} \psi_{6\sigma} + h.c.)$$

$$B_{\bigcirc} = \sum_{\sigma} (\psi_{1\sigma}^{\dagger} \psi_{6\sigma} + \psi_{5\sigma}^{\dagger} \psi_{4\sigma} + \psi_{3\sigma}^{\dagger} \psi_{2\sigma} + h.c.) \qquad (2)$$

Here 1, 2, ..., 6 are the six sites of a hexagon arranged in clockwise order.

When P is large  $H_1$  favors the Kekule VBS order shown in Fig. 2. Such interaction can be generated by integrating out the optical phonon associated with the Kekule distortion. Remarkably, the model Eq. (1) is amendable to QMC simulation without sign problems at any filling factor![23–26] (See section II. of the SM for details.[30]) Note that the interaction in Eq. (1) is different from that used in Ref. [27]. Under the interaction used in Ref. [27] weak VBS order only appears in a small parameter regime. In contrast, the plaquette interaction in Eq. (1) favors strong VBS order in a wide parameter regime, making the investigation of superconductivity and non-Fermi-liquid behavior emerging from the doped VBS phase much easier.

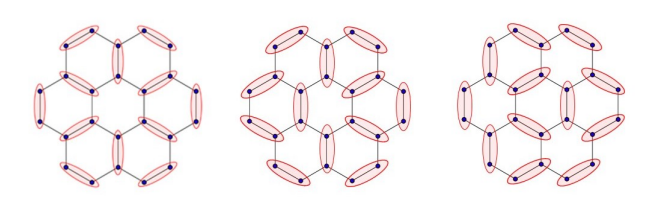


FIG. 2. The three-fold degenerate Kekule valence bond solid ground state.

To study the effects of repulsive interaction we add the Hubbard interaction

$$H_2 = U \sum_{i} \left( n_{i\uparrow} - \frac{1}{2} \right) \left( n_{i\downarrow} - \frac{1}{2} \right) \tag{3}$$

to Eq. (1) in later part of the paper. With  $H_2$  the model is sign-problem-free only at half-filling. However, for honeycomb lattice at low doping, the sign problem is not severe. This is because of the low density of states associated with the doped Dirac cone. This allows us to simulate down to relatively low temperatures.

#### Half filling

First, we study the ground state properties of Eq. (1) at half-filling. This is achieved by performing projector QMC simulation. (See section I. of the SM for the details of the simulation.[28]) For small P the four-fermion interaction is an irrelevant perturbation to the Dirac semimetal phase in the renormalization group sense. In this phase there are gapless particle-hole excitations at the Dirac nodes  $\vec{K} = (\frac{4\pi}{3}, 0)$  and  $\vec{K'} = (-\frac{4\pi}{3}, 0)$ . For large P the four-fermion interaction,  $H_1$ , triggers the formation of the insulating Kekule VBS phase shown in Fig. 2. To quantify the VBS order we compute VBS structure factor  $S(\vec{Q}, L)$ , i.e., the Fourier transform of VBS order parameter correlation function at the ordering wavevector  $\vec{Q} = \vec{K}$  and  $\vec{K'}$ . To determine the critical value of P we compute the "RG invariant ratio"

$$R(P,L) = \frac{S(\vec{Q}, P, L)}{S(\vec{Q} + \delta \vec{q}, P, L)} - 1,$$

where  $\delta \vec{q} = (0, \frac{4\pi}{\sqrt{3}L})$  is the momentum closest to  $\vec{Q}$  on a finite honeycomb lattice with linear dimension L. (See

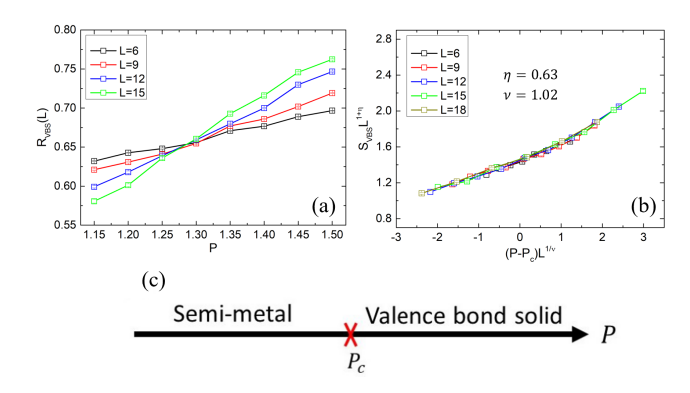


FIG. 3. (a) The RG invariant ratio  $R(P,L) = \frac{S(\vec{Q},P,L)}{S(\vec{Q}+\delta\vec{q},P,L)} - 1$  as a function of P for different L. The crossing of different L value curves marks the critical  $P_c \approx 1.28$ . (b) The finite size-scaling plot of  $L^{1+\eta}S(\vec{Q},P,L)$  versus  $L^{1/\nu}(P-P_c)$  where the value of  $\eta \approx 0.63$  and  $\nu \approx 1.02$  are the anomalous dimension of the VBS order parameter and the correlation length exponent, respectively. (c) The zero-temperature phase diagram at half-filling. The statistical errors of QMC simulation are indicated by error bars, which are even smaller than the sizes of data points in this figure.

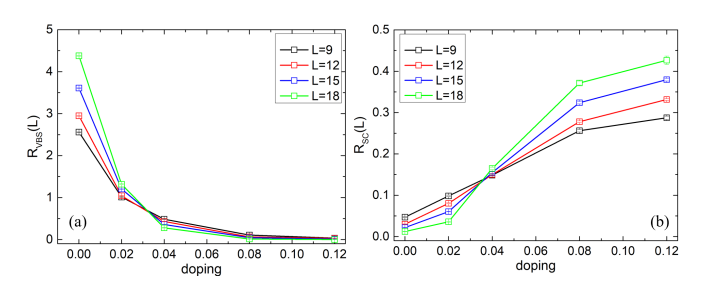


FIG. 4. The RG-invariant ratio associated with the (a) VBS and (b) SC order as a function of doping for several values of L at zero temperature.

section III. of the SM for more details.[31]) In the VBS ordered phase we expect R(P,L) to diverge as  $L \to \infty$ , while for the disordered phase R(P,L) should vanish with increasing L. At the critical point  $P=P_{\rm c}$ , due to the divergence of the correlation length, we expect  $R(P_{\rm c},L)$  to be independent of L.

The results for R(P,L) are shown in Fig. 3(a), from which we estimate  $P_{\rm c}\approx 1.28$ . Naively one might expect the 3-fold anisotropy of VBS order will render the order-disorder transition first order, as what happens in the 3-state Potts model. However, in the present situation, the disordered phase is Dirac semimetal (DSM) and recent studies show that due to the coupling to gapless fermions there is emergent U(1) symmetry at the DSM-VBS transition. As a result, the transition is continuous and belongs to the chiral-XY universality class [29]. In Fig. 3(b) we perform finite-size scaling to determine the anomalous dimension of order parameter  $\eta$  and the correlation length exponent  $\nu$ , which agrees with previous studies [29].

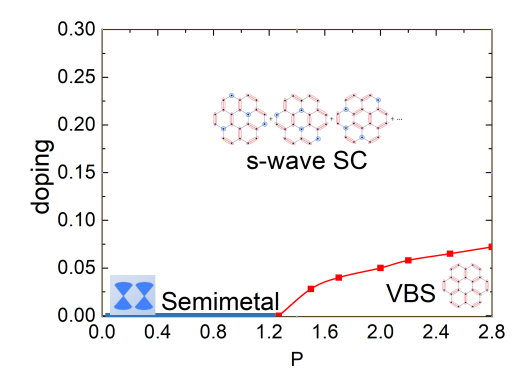


FIG. 5. The numerical zero-temperature phase diagram of Eq. (1).

#### Superconductivity at non-zero doping

In this section, we show superconductivity emerges from the VBS phase upon doping. We consider the two most probable spin-singlet pairing symmetry: s and d+id. (On the honeycomb lattice d-wave pairing forms a two-dimensional  $(d_{x^2-y^2}, d_{xy})$  irreducible representation of the lattice rotation group.) While the doping density is fixed by the trial wavefunction in zero-temperature simulation, in finite temperature QMC it is fixed by the chemical potential. In section IV. of the SM[32], we show the doping density versus the chemical potential for several interaction parameters.

Fixing P at 1.6, which places the system in the VBS phase at half filling, we study the VBS and SC orders as a function of doping density, n, at zero temperature. Within the numerical uncertainty, the vanishing of the VBS order occurs simultaneously with the onset of an s-wave SC order. Moreover, the crossing of the RG invariant ratios suggests the transition is continuous. The crossing point of the RG-invariant ratios in Fig. 4(a) and (b) places the critical doping within (0.03, 0.035). In Fig. 5 we show the zero-temperature phase diagram.

Of course, there is always the possibility that the VBS-SC transition is weakly first order with a correlation length exceeding the largest system size we studied. Moreover, if the transition is indeed continuous it would constitute an example of Landau-forbidden transition. A more thorough analysis of the phase transition awaits future studies.

To study the normal to superconducting phase transition as a function of temperature we calculate the SC susceptibility (see section III. of SM for details[31]) using the finite-temperature QMC technique. The SC transition temperature  $T_c$  is determined by studying the finite size scaling behavior of the SC susceptibility. The result suggests the transition is in the Kosterlitz-Thouless universality class. At the critical temperature, the finite size scaling behaviour of the SC susceptibility is

$$\chi_{\rm SC}(T_{\rm c},L) \sim L^{2-\eta}$$
, where  $\eta = 0.25$ .

For P = 1.6 and doping level n = 0.1, we plot the scaled SC susceptibilities versus the inverse temperature for several system sizes in Fig. 6.

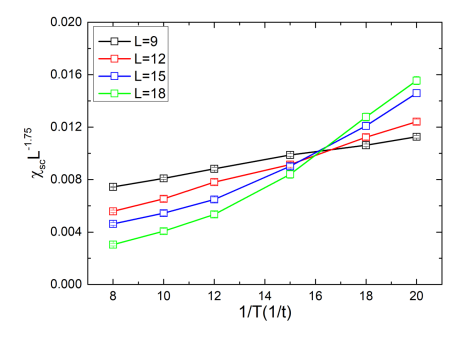


FIG. 6. The scaled SC susceptibility versus the inverse temperature for different values of L. The crossing point marks the  $T_c$  of the Kosterlitz-Thouless transition. The plaquette interaction strength is fixed at P=1.6 and doping level is n=0.1.

The crossing point of different L curves marks the Kosterlitz-Thouless  $T_c$ . Using this procedure, we estimate  $T_c$  as a function of P for doping n=0.1. The result is shown in shown as the black squares in Fig. 7. The maximum  $T_c$  is about 0.06.

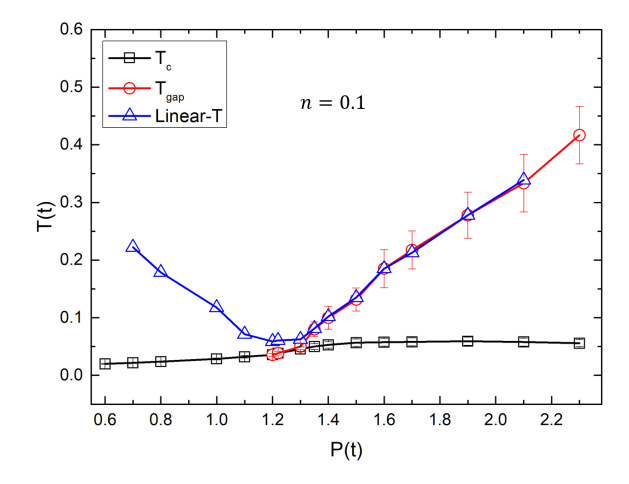


FIG. 7. The numerical P-T phase diagram at doping level n=0.1 for  $0.6 \leq P \leq 2.3$ . The black square marks the Kosterlitz-Thouless SC phase transition. In the region above the curve marked by the blue squares, the resistivity exhibits linear-T behavior. Below the curve marked by the red circles, a pseudogap opens.

### The pseudogap and non-Fermi liquid transport behavior

When the temperature drops below a certain crossover scale  $T^*$ , the short-range VBS correlation sets in. This is accompanied by the opening of a (pseudo) single-particle gap. For low doping, the SC phase coherence sets in at a significantly lower temperature due to the low superfluid density. This is shown in Fig. 8 for P=1.6 and n=0.1.

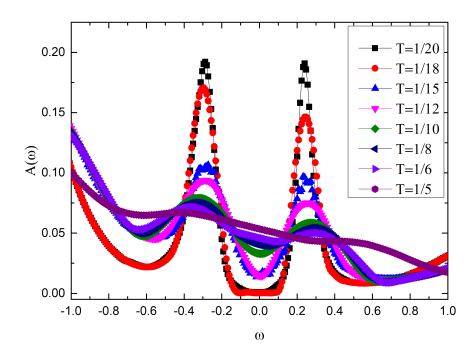


FIG. 8. The single-particle spectral function versus  $\omega$  for different temperatures. The interaction strength is P=1.6 and doping level is n=0.1. The linear system size is L=15. The  $T_c$  is approximately 1/17, and the single-particle gap opening temperature  $T_{\rm gap}$  is estimated to be 1/6.

The details of how to calculate the single-particle spectral function via analytical continuation [33] are discussed in section V. of the SM[34]. In Fig. 7 the curve marked by the red circles mark the crossover temperatures  $T^*$  below which the pseudogap opens. When P is larger than the critical value of the VBS phase at half-filling, pseudogap exists in a wide temperature range. This supports the origin of the pseudogap being the short-range VBS correlation.

Because transport near quantum critical points often exhibits non-Fermi liquid behavior, in the following we study the resistivity when P is fine-tuned near the critical value separating the semimetal and VBS phases at half filling. We calculate the dc resistivity by computing the imaginary-time current-current correlation function  $\Lambda(\tau) = \langle j_{\mu}(\tau)j_{\mu}(0)\rangle$ , where  $j_{\mu}$  is the  $\vec{q}=0$  component of the current operator in  $\mu=x$  or y direction. The optical conductivity is related to  $\Lambda(\tau)$  by

$$\Lambda(\tau) = \int_0^\infty \frac{d\omega}{\pi} \frac{\omega e^{-\tau\omega}}{1 - e^{-\beta\omega}} \sigma(\omega),$$

with  $\beta$  being the inverse temperature. To deduce the dc resistivity we use the relation

$$\rho = \pi T^2 \Lambda (\beta/2)^{-1}$$

in Ref.[35, 36]. In Fig. 9, we show the results for doping level n=0.1. Interestingly, the resistivity obeys a linear-T behavior in a significant temperature window when P is close to  $P_c$ . When P is significantly less than  $P_c$ , the temperature dependence is consistent with the conventional  $T^2$  behavior. For  $P>P_c$ , the resistivity exhibits an upturn at low temperatures, due to the opening of the pseudogap in Fig. 8. For a clean system such as the one in our study, the resistivity is due to the Umklapp scattering.

#### The effects of Hubbard interaction

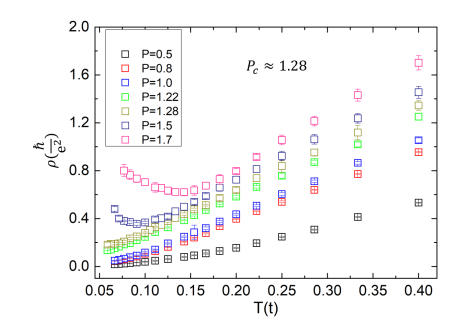


FIG. 9. Resistivity versus temperature for several values of P near the critical values  $P_{\rm c}\approx 1.28$  for the semimetal to VBS quantum phase transition at half filling. The linear system size is L=15.

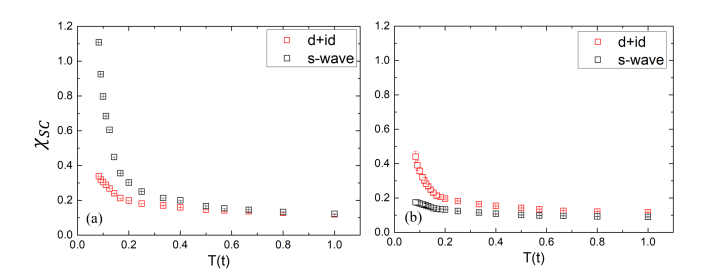


FIG. 10. The s and d+id-wave SC susceptibilities as a function of temperature with fixed Plaquette interaction P/t=1.5 and Hubbard interaction strength (a) U/t=0 and (b) U/t=2. Due to the reappearing of the sign problem we only managed to get low-temperature data for linear system size L=6.

In the presence of the Hubbard interaction (Eq. (3)) the sign problem reappears at non-zero doping. However, on the honeycomb lattice, it is not too severe due to the low density of states associated with the doped Dirac cone. However, given a system size, the sign problem does limit how low we can go in temperature. In Fig. 10 we compare the s and d+id-wave SC pairing susceptibilities for two values of U. For U/t=0 the s-wave pairing dominates. When we increase U/t to 2 the d+id susceptibility surpasses the s-wave one and exhibits "divergent" behavior in the temperature range we have studied. In section VI. of the SM, we show a Curie-Weiss fit of the d+id SC susceptibility which further corroborates that d+id SC susceptibility is divergent at zero temperature, at least for the system sizes we studied[37]. This result suggests that when the Hubbard interaction is sufficiently strong the SC emerging from the doped VBS phase is a chiral superconductor!

#### Conclusion

Our approximation-free QMC simulation suggests that when holes are doped into a valence bond solid insulator superconductivity may emerge. We believe this is because the mobile holes displace the valence bonds, which in turn suppresses the valence bond solid order. We have also shown that the short-range repulsive interaction can change the pairing symmetry of superconductivity. In this work, we come across several interesting phenomena including the pseudogap, and non-Fermi liquid transport behavior, which bear resemblance to the cuprates.

Acknowledgements: This work was primarily funded by the U. S. Department of Energy, Office of Science, Office of Basic Energy Sciences, Materials Sciences and Engineering Division under Contract No. DE-AC02-05-CH11231 (Theory of Materials program KC2301). This research is also funded in part by the Gordon and Betty Moore Foundation.

- \* Corresponding author: dunghai@berkeley.edu
- [1] P. W. Anderson, Science **235**, 1196 (1987).
- [2] S. A. Kivelson, D. S. Rokhsar, and J. Sethna, Phys. Rev. B 35, 8865 (1987).
- [3] P. A. Lee, N. Nagaosa, and X.-G. Wen, Rev. Mod. Phys. 78, 17 (2006).
- [4] L. Balents, Nature **464** 199 (2010).
- [5] M. R. Norman, Rev. Mod. Phys. 88, 041002 (2016).
- [6] Y. Zhou, K. Kanoda, and T.-K. Ng, Rev. Mod. Phys. 89, 025003 (2017).
- [7] C. Broholm, R. J. Cava, S. A. Kivelson, D. G. Nocera, M. R. Norman, T. Senthil, Science 367, 6475 (2020).
- [8] A. Kitaev, Annals of Physics **321**, 2 (2006).
- [9] R. Moessner and S. L. Sondhi, Phys. Rev. Lett. 86, 1881 (2001).
- [10] H. Yao and D.-H. Lee, Phys. Rev. Lett. 107, 087205 (2011).
- [11] H.-C. Jiang and S. A. Kivelson, Phys. Rev. Lett. 127, 097002 (2021).
- [12] N. Read and S. Sachdev, Phys. Rev. B 42, 4568 (1990).
- [13] A. W. Sandvik, Phys. Rev. Lett. 98, 227202 (2007).
- [14] T. C. Lang, Z. Y. Meng, A. Muramatsu, S. Wessel, and F. F. Assaad, Phys. Rev. Lett. 111, 066401 (2013).
- [15] P. G. Radaelli, Y. Horibe, M. J. Gutmann, H. Ishibashi, C. H. Chen, R. M. Ibberson, Y. Koyama, Y.-S. Hor, V. Kiryukhin and S.-W. Cheong, Nature 416, 155 (2002).
- [16] Y. Okamoto, S. Niitaka, M. Uchida, T. Waki, M. Taki-gawa, Y. Nakatsu, A. Sekiyama, S. Suga, R. Arita, and H. Takagi Phys. Rev. Lett. 101, 086404 (2008).

- [17] K. Matan, K. Matan, T. Ono, Y. Fukumoto, T. J. Sato, J. Yamaura, M. Yano, K. Morita and H. Tanaka, Nature Phys. 6, 865 (2010).
- [18] Y. Shimizu, H. Akimoto, H. Tsujii, A. Tajima, and R. Kato, Phys. Rev. Lett. 99, 256403 (2007).
- [19] J. P. Sheckelton, J. R. Neilson, D. G. Soltan, and T. M. McQueen, Nat. Mater. 11, 493 (2012).
- [20] C. Gutiérrez, C.-J. Kim, L. Brown, T. Schiros, D. Nord-lund, E. B. Lochocki, K. M. Shen, J. Park, and A. N. Pasupathy, Nat. Phys. 12, 950 (2016).
- [21] R. W. Smaha, W. He, J. M. Jiang, J. Wen, Y. F. Jiang, J. P. Sheckelton, C. J. Titus, S. G. Wang, Y. S. Chen, S. J. Teat, A. A. Aczel, Y. Zhao, G. Xu, J. W. Lynn, H. C. Jiang, and Y. S. Lee, npj Quantum Mater. 5, 23 (2020).
- [22] F.F. Assaad, and H. G. Evertz. "World-line and determinantal quantum Monte Carlo methods for spins, phonons and electrons" in Computational Many-Particle Physics. Springer, Berlin, Heidelberg, 2008. 277-356.
- [23] F. F. Assaad, Phys. Rev. B 71, 075103 (2005).
- [24] C. Wu, S. -C. Zhang, Phys. Rev. B 71, 155115 (2005).
- [25] Z. -X. Li, Y. -F. Jiang, H. Yao, Phys. Rev. B 91, 241117 (2015).
- [26] Z. -X. Li, Y. -F. Jiang, H. Yao, Phys. Rev. Lett. 117, 267002 (2016).
- [27] Z.-X. Li and H. Yao, Annual Review of Condensed Matter Physics 10, 337 (2019).
- [28] See Supplemental Material at \*\*\* for the details of QMC simulation.
- [29] Z.-X. Li, Y.-F. Jiang, S.-K. Jian and H. Yao, Nature Communications 8, 314 (2017).
- [30] See Supplemental Material at \*\*\* for the absence of sign problem in model Eq. (1).
- [31] See Supplemental Material at \*\*\* for the defination of SC structure factor, correlation length ratio and SC susceptibility.
- [32] See Supplemental Material at \*\*\* for the doping dependence on the chemical potential.
- [33] A. W. Sandvik, Phys. Rev. B **57** 10287 (1998).
- [34] See Supplemental Material at \*\*\* for the details of analytical continuation.
- [35] S. Lederer, Y. Schattner, E. Berg, and S. A. Kivelson, Proc. Natl. Acad. Sci. USA 114, 4905 (2017).
- [36] E. W. Huang, R. Sheppard, B. Moritz, T. P. Devereaux, Science 366, 987 (2019).
- [37] See Supplemental Material at \*\*\* for the Curie-Weiss fit of the d+id SC susceptibility.